



ELSEVIER

Available online at www.sciencedirect.com

SCIENCE @ DIRECT®

Journal of Geodynamics 39 (2005) 61–77

JOURNAL OF
GEODYNAMICS

<http://www.elsevier.com/locate/jog>

The 2001 $M_w = 6.4$ Skyros earthquake, conjugate strike-slip faulting and spatial variation in stress within the central Aegean Sea

A. Ganas^{a,*}, G. Drakatos^a, S.B. Pavlides^b, G.N. Stavrakakis^a, M. Ziazia^a,
E. Sokos^a, V.K. Karastathis^a

^a *Institute of Geodynamics, National Observatory of Athens, P.O. Box 20048, Lofos Nimfon, 118 10 Athens, Greece*

^b *Department of Geology, Aristotle University of Thessaloniki, Thessaloniki 54124, Greece*

Received 5 February 2004; received in revised form 30 August 2004; accepted 11 September 2004

Abstract

This paper uses the seismological data provided by analysis of the July 26, 2001 Skyros earthquake ($M_w = 6.4$) aftershock sequence to discuss various models for Quaternary deformation of the central Aegean region. In particular, it is suggested that the left-lateral Skyros fault is a primary strike-slip fault formed in Early Quaternary times and striking perpendicular to the right-lateral North Anatolian Fault (NAF). This fault blocks linkage between normal faults offshore Evia Island and NAF. The fault kinematics, stress transfer analysis and available focal mechanisms indicate that the stress field is characterized by a switch between vertical σ_2 and vertical σ_1 with σ_3 trending roughly $N10^\circ E$. The spatial variation of the stress field is imposed by the N–S, extensional strain due to conjugate strike slip faulting. The variation in stress defines a 170 km wide area from $23^\circ E$ to $25^\circ E$ comprising the terminating influence of the 1200 km long North Anatolian Fault on to the north-central Aegean crust.

© 2004 Elsevier Ltd. All rights reserved.

Keywords: Conjugate fault; Strike-slip; Focal mechanism; Stress tensor; Stress transfer; Aegean

1. Introduction

On July 26, 2001 at 00:21:39 GMT a strong earthquake of magnitude $M_w = 6.4$ hit the central Aegean Sea (Fig. 1; Melis et al., 2001; Drakatos et al., 2004; Roumelioti et al., 2004). This earthquake occurred along a NW–SE, left-lateral fault, offshore Skyros Island (Fig. 1; Benetatos et al.,

* Corresponding author.

E-mail address: aganas@gein.noa.gr (A. Ganas).

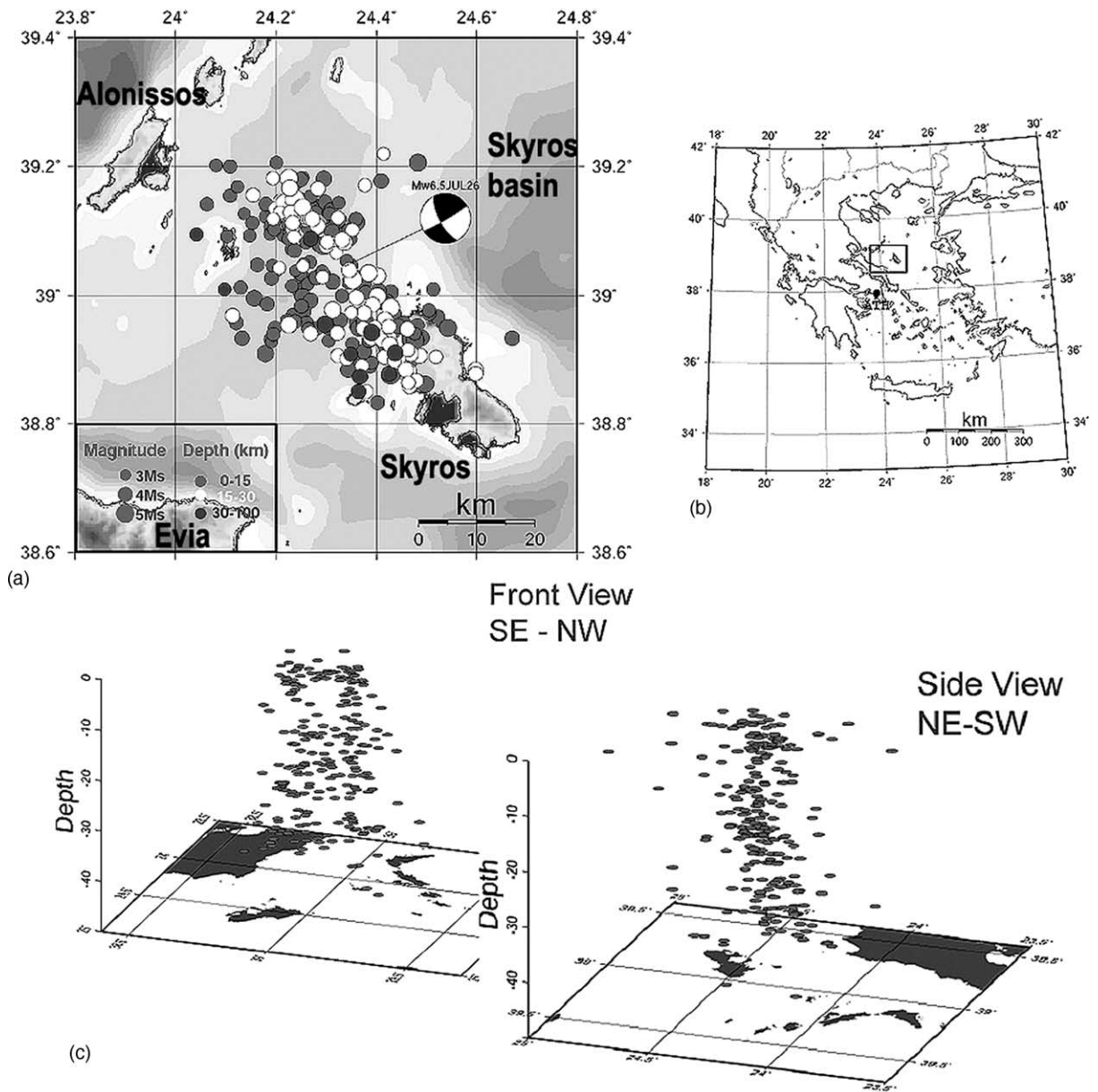
SKYROS EQ AFTERSHOCKS (N=263 > 3.3 Ms - RMS < 0.8 s) from NOAGI network


Fig. 1. (a) Map of epicentres of the Mw 6.4 Skyros earthquake aftershock sequence, recorded by NOA (from Drakatos et al., 2004). Note that mainshock epicentre is located at the middle of the rupture zone. Two hundred sixty three events are shown for which the R.M.S.error < 0.8 s and their surface magnitude Ms > 3.3. (b) The regional setting of Skyros. (c) 3D perspective views of the aftershock sequence both along (NW–SE) and across (NE–SW) the rupture zone.

2002; Karakostas et al., 2003). The kinematics of this fault pose several questions on the mode of crustal deformation in that area because the central Aegean Sea region is regarded as a typical right-lateral strike-slip faulting regime (e.g. Taymaz et al., 1991; Pavlides and Tranos, 1991; Papadopoulos et al., 2002; Kiratzi and Louvari, 2003). These questions are related to (a) the strain accommodation in central Aegean, (b) stress axes orientations across the Aegean and (c) the westward propagation of the north Anatolian Fault into the Aegean during Quaternary (e.g., Armijo et al., 1999). Notably, this is the first large earthquake in the Skyros area showing that significant strain is accommodated by slip along left-lateral fault planes. The role of such faults may be more important than what was previously considered as they are capable of hosting earthquakes of magnitude 6–7.

The main contribution of this work is to establish the present-day stress field near the island of Skyros (Fig. 1), the July 26, 2001 rupture zone dimensions, and the geometry and kinematics for the seismic fault. We also investigate the role of the Skyros fault in central Aegean tectonics. Our analysis examines both age and dimensions of the Skyros fault and its behaviour with finite strain. We also examine if accumulation of slip along the Skyros fault throughout Quaternary has led to its rotation towards the finite extension direction, as commonly observed in regions of strike-slip faulting (e.g. Nur et al., 1986). In terms of the regional stress field we apply stress tensor analysis and stress transfer analysis in combination with published focal mechanism data in order to understand its spatial variation. Central Aegean is subjected to both East–West directed compression (e.g. Taymaz et al., 1991) and to N–S extension as manifested by the opening of several basins (e.g. Koukouvelas and Aydin, 2002). It is interesting to map this stress field variation in view of the new data provided by the July 26, 2001 earthquake. The stress field stops to vary as we cross the landmass of Evia where faulting is mainly extensional (Roberts and Ganas, 2000; Kiratzi, 2002).

2. Seismological data

The July 26, 2001 earthquake and its aftershocks were well recorded by the National Observatory of Athens (NOA) network. A summary of the source parameters proposed by NOA and other institutions is given in Table 1. The analysis of digital waveforms from 17 broadband stations indicates that the earthquake ruptured a strike-slip fault oriented N150°E, and dipping 65–70° to the southwest (Melis et al., 2001; Drakatos et al., 2004). Almost all computed solutions by other workers suggest that the slip vector rake plunges approximately 10–20° upwards, i.e. indicating a reverse component (Table 1). Our analysis of 263 well recorded aftershocks show that the events are vertically distributed down to a depth of almost 30 km which is the estimated Moho depth (Makris and Veis, 1977; Tsokas and Hansen, 1997). The aftershock sequence orientation (NW–SE) defines clearly the left-lateral kinematics of the rupture (Fig. 1). The deeper events of the aftershock sequence are located towards the hanging-wall (i.e. to the SW of Skyros island; Fig. 1), a feature that may correspond to motion along a low-angle shear zone in the lower crust.

The focal mechanisms and *T*-axes data from 50 well-determined focal mechanisms of the aftershock sequence are presented in Figs. 2 and 3, respectively. The focal mechanisms of the aftershock sequence originate from analysis of first-motion polarities of P-waves using the HypoInverse and FPFIT software packages and are presented in Table 2. On July 21 two foreshocks occurred within 5 km from the epicentre of the mainshock, followed by another foreshock on July 25. The majority (41 out of 50) of analysed

Table 1

Focal parameters and fault-plane solutions published for the July 26, 2001 earthquake, offshore Skyros

Origin	φ (°N)	λ (°E)	D (km)	M	M_0 (nm) $\times 10^{18}$	U (m)	L (km)	ξ (°) NP1 NP2	δ (°) NP1 NP2	λ (°) NP1 NP2
NOAGI (Drakatos et al., 2004)	39.046	24.338	16.9	Ms = 5.8 Mw = 6.5	4			160	70	20
USGS Web-page	39.06	24.34	14	Mw = 6.5 Mb = 6.0 Ms = 6.6	5.4			145 55	85 86	4 175
CSEM (GFZ sol)	39.07	24.14	10	Mw = 6.4	5.2			128 37	81 84	6 171
HRV CMT web-page	38.96	24.29	15	Mw = 6.4	5.4			148 238	76 89	-1 -166
Karakostas et al., 2003				Mw = 6.4			23			
Zahradnik (2002)			8	Mw = 6.5	4.1	0.63	16–24	150	70	10
Benetatos et al., 2002	38.99	24.38	12	Mw = 6.5	5.98	0.30	32	151 60	83 84	7 173

Epicentre coordinates are in geographical degrees, D is hypocentral depth, M_0 is seismic moment, U is coseismic displacement, L is rupture length, and ξ , δ , λ are strike, dip and rake, respectively. NP1 and NP2 indicate nodal plane parameters.

events define a 35 km long and 10 km wide rupture zone that grew rapidly along strike. During the first hour the aftershocks occupied a 19 km long zone while in 24 h the rupture zone was extending for 28 km (Fig. 2). The T -axes are aligned in a general, N–S direction with a mean azimuth of N7°E (Fig. 3). The T -axes orientation indicates N–S extensional strain. The same orientation has been proposed for the 1967, normal faulting event inside the Skyros basin (Fig. 1; Taymaz et al., 1991). We also note that, the seismologically determined extension direction around Skyros agrees with geological data from the Gulf of Evia graben, located 70 km to the west (Fig. 1, Fig. 7 below). The geological data comprise sets of measurements of slip directions along fresh fault surfaces around the Evia rift, where it was found that the mean extension axis is directed N14°E (Roberts and Ganas, 2000). Similar orientations (N10°E) are reported by Caputo and Pavlides (1993) for the area of Thessaly, 150 km to the NW of Skyros.

We also used the focal parameters of the 50-well determined shocks to perform stress tensor inversion (Fig. 4). The inversion method we applied to achieve the best fitting stress model is the one provided by Gephart and Forsyth (1984) and Gephart (1990). The method's main assumption is that the deviatoric stress tensor is uniform over the region of study. Other assumptions are that the slip vector of any focal mechanism points in the direction of the maximum resolved shear stress on the fault plane and the earthquakes are shear dislocations on pre-existing faults. In order to obtain successful results by the inversion it is necessary for the input dataset to include at least four different orientations of focal mechanisms (Gephart and Forsyth, 1984). The aim of the inversion is to determine the directions of the principal stress axes σ_1 , σ_2 , σ_3 ($\sigma_1 > \sigma_2 > \sigma_3$) and the shape factor $R = (\sigma_2 - \sigma_1) / (\sigma_3 - \sigma_1)$ which indicates the

Table 2

Focal plane solution of the 50 well-determined shocks of the Skyros earthquake sequence (3 foreshocks–47 aftershocks)

ID	Date	Latitude	Longitude	Depth	Strike 1st pl.	Dip	Rake	Strike Aux. pl.	Dip	Rake	Mag.
1	721	39.071	24.318	20.89	135	40	−20	240	77	−128	4.6
2	721	39.065	24.387	3.50	130	60	0	40	90	150	5.1
3	725	39.082	24.349	7.32	245	75	−170	152	80	−15	4.7
4	726	39.025	24.359	13.79	155	75	−30	253	61	−163	5.3
5	726	39.107	24.309	9.55	100	55	−50	224	51	−132	4.8
6	726	38.965	24.431	7.87	0	60	50	239	48	−138	4.9
7	726	39.112	24.283	19.47	100	70	−50	212	43	−150	4.9
8	726	39.078	24.308	29.34	135	85	10	44	80	175	5.0
9	726	38.949	24.412	28.58	55	90	−140	325	50	0	5.2
10	726	38.929	24.470	11.87	230	85	170	320	80	5	5.3
11	726	39.035	24.384	17.85	300	85	0	210	90	175	4.7
12	726	38.999	24.402	17.75	125	85	−30	217	60	−174	4.7
13	726	38.937	24.391	28.28	60	85	−160	328	70	−5	5.1
14	726	38.907	24.487	21.29	125	55	110	272	39	64	4.2
15	726	38.986	24.392	27.95	325	90	10	235	80	180	4.3
16	726	39.010	24.514	10.63	15	30	20	267	80	118	4.2
17	726	39.067	24.320	29.75	240	55	170	335	81	35	4.1
18	726	39.076	24.293	6.20	245	60	180	330	90	30	4.3
19	726	38.944	24.404	26.07	325	85	0	235	90	175	4.8
20	726	38.943	24.390	30.20	55	90	−140	325	50	0	4.6
21	726	39.025	24.353	27.16	55	90	−140	325	50	0	5.1
22	726	39.111	24.284	18.97	130	40	0	40	90	130	4.3
23	726	39.018	24.373	6.09	60	90	−150	330	60	0	4.5
24	726	39.083	24.336	19.10	220	85	−170	129	80	−5	4.5
25	726	39.125	24.258	16.19	115	70	−30	216	61	−157	5.1
26	726	38.962	24.417	25.23	60	90	−160	330	70	0	4.5
27	726	38.910	24.469	26.27	330	90	30	240	60	180	4.4
28	727	38.862	24.498	6.39	50	85	−140	315	50	−6	4.8
29	728	38.901	24.440	29.95	60	90	−130	330	40	0	5.1
30	730	39.126	24.244	19.68	140	85	−70	243	20	−166	4.4
31	730	39.119	24.233	22.11	110	85	0	20	90	175	4.3
32	730	39.181	24.295	13.65	325	80	−50	66	41	−165	4.4
33	730	39.114	24.360	9.11	160	70	−30	261	61	−157	4.8
34	731	38.876	24.425	32.50	170	60	−30	276	64	146	4.3
35	82	39.206	24.483	7.41	120	65	30	16	63	151	4.8
36	83	38.996	24.157	7.95	90	80	120	196	31	19	4.4
37	83	39.117	24.268	14.89	330	90	30	240	60	180	4.4
38	83	39.098	24.272	13.93	150	85	−50	245	40	−172	4.0
39	88	38.931	24.478	12.52	50	70	−140	303	52	−25	4.9
40	810	38.991	24.263	10.33	145	75	30	46	61	163	4.6
41	812	38.999	24.253	6.64	150	75	−30	248	61	−163	4.4
42	827	39.137	24.253	21.93	45	75	−150	306	61	−17	4.8
43	94	38.941	24.269	18.66	315	85	−10	45	80	−175	4.0
44	97	38.955	24.226	24.87	325	85	0	235	90	175	4.5
45	910	38.960	24.223	12.26	330	90	30	240	60	180	4.1
46	919	38.949	24.459	13.89	345	70	60	224	35	144	4.3
47	107	38.953	24.443	13.23	110	65	−70	249	31	−126	4.0
48	1012	39.176	24.239	13.87	320	80	10	228	80	169	4.3
49	1029	38.877	24.428	13.70	75	75	−150	336	61	−17	5.3
50	1029	38.874	24.367	33.30	85	85	−140	350	50	−6	4.2

Strike is measured clockwise from North. Rake values >0 mean reverse slip component. Mag., is surface magnitude.

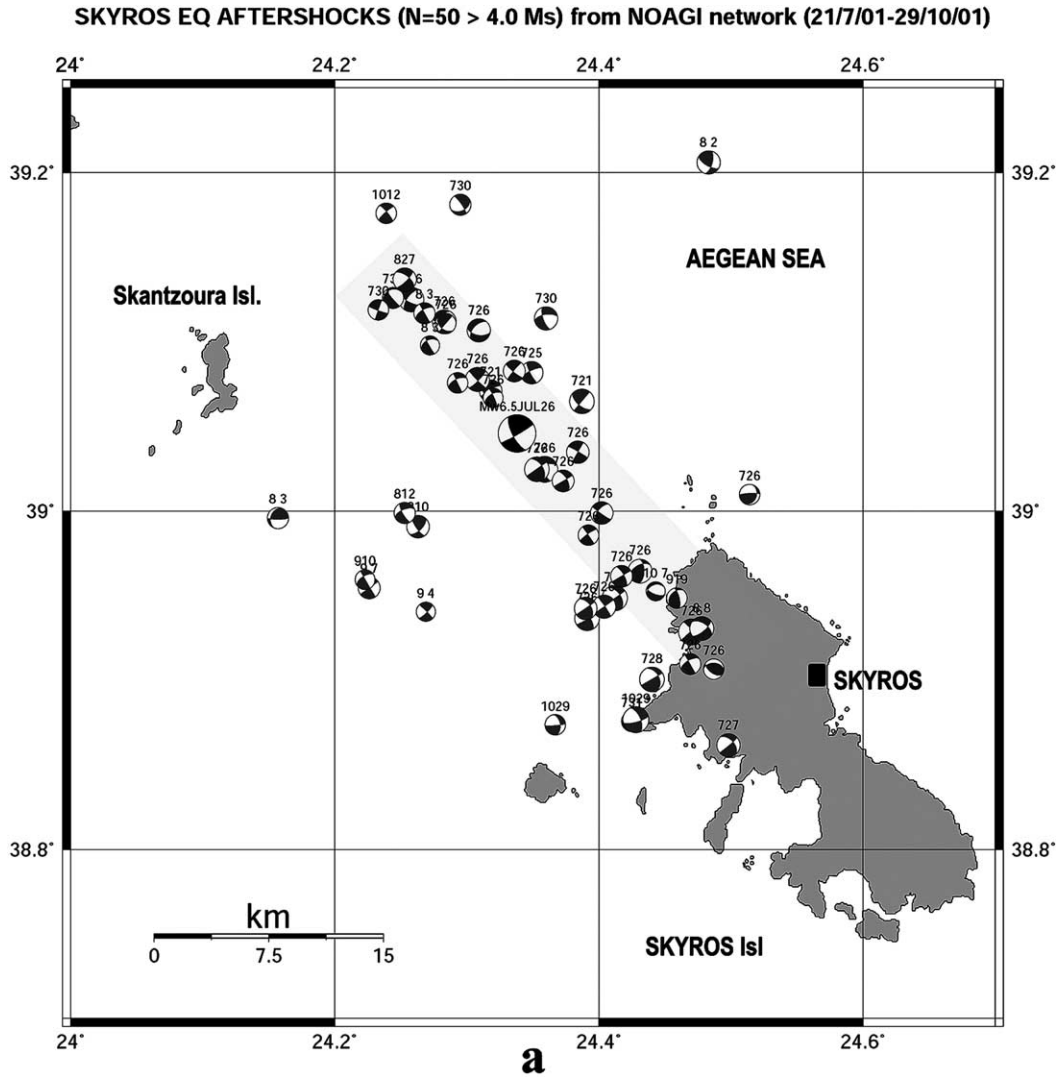


Fig. 2. Map of focal mechanisms of the aftershock sequence reported in Table 2. Equal-area, lower hemisphere projections of fault planes with black indicating compressional quadrant. Note that strike slip faulting predominates. Text above each mechanism indicates event date (month/day).

magnitude of σ_2 relative to σ_1 and σ_3 . The processing was carried out using the ZMAP software (Wiemer and Zuniga, 1994). We found that the maximum compressive stress σ_1 is sub-horizontal, oriented ESE–WNW (plunge 9° , azimuth $N282^\circ E$) while the least compressive stress σ_3 is horizontal, oriented N–S (plunge 7° , azimuth $N13^\circ E$). The stress ratio R has a value of 0.6 (Fig. 4). The angular difference (misfit) between the computed and the observed slip direction is 5.8° , thus assuring the best fitting stress model. The results of the stress tensor inversion confirm the $N7^\circ E$ extension direction suggested by the mean T -axis.

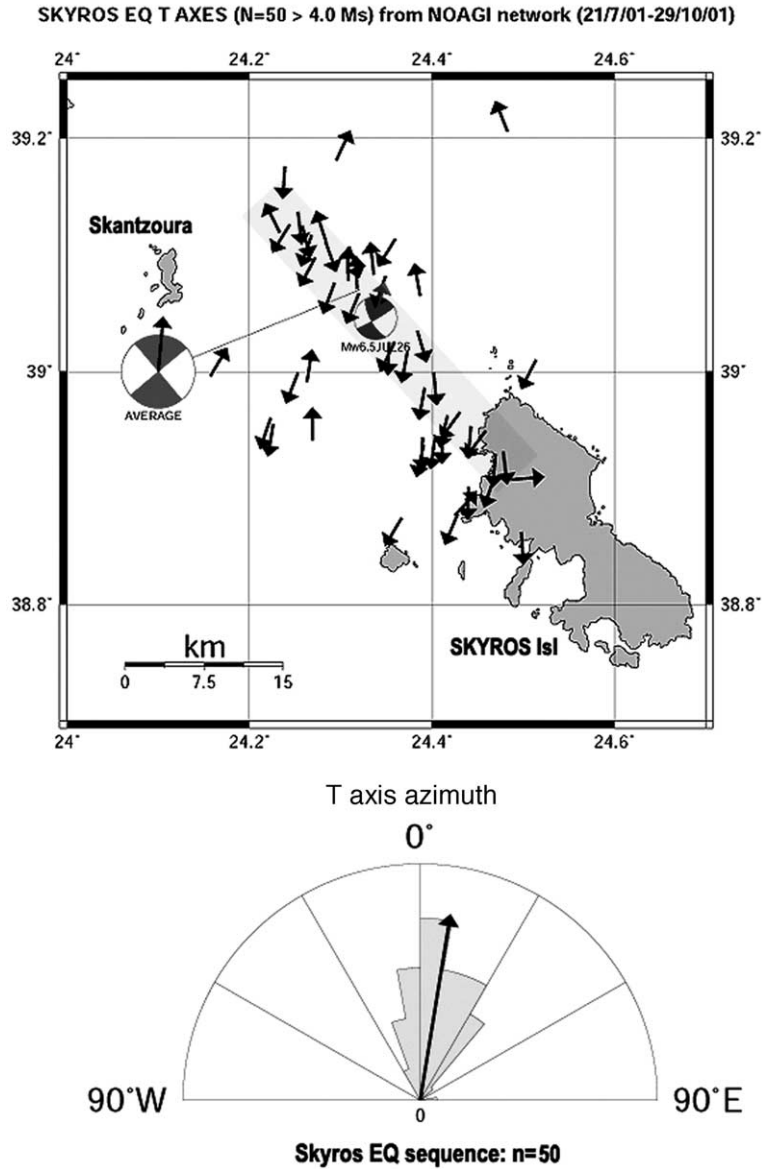


Fig. 3. (Top) Map of *T*-axis orientations of focal mechanisms reported in Table 2 and shown in Fig. 2. The *T*-axis of the mainshock is also shown together with its focal mechanism. (Bottom) The rose diagram of the population with the mean vector directed to N7°E.

In addition, our aftershock analysis shows an interesting feature of seismicity. The NE–SW cross-section through the aftershock sequence reveals a V-shaped pattern of seismicity (Fig. 5). Several aftershock clusters inside this V-shaped envelope of seismicity may be defined which may be correlated with secondary faulting within the major, strike-slip fault zone. In addition, seismicity is mostly concentrated in the western side of the fault.

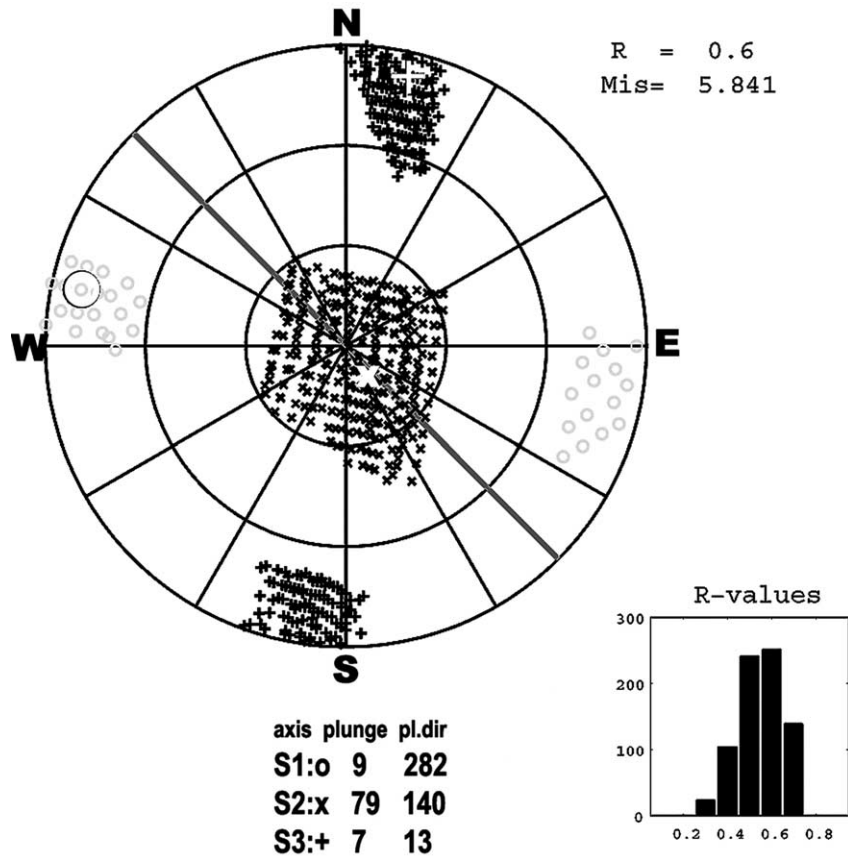


Fig. 4. Stress tensor inversion analysis of the aftershock sequence. Crosses on stereonet indicate σ_3 orientation, X σ_2 and circles σ_1 orientation, respectively. Numbers indicate mean values of the populations. R is the stress ratio. Mis indicates slip vector misfit rotation angle (in degrees) relative to the best stress model. The histogram shows the distribution of R . See text for discussion.

3. Co-seismic Coulomb stress changes

The stress transfer analysis is not intended to reproduce aftershock epicentre maps as in Stein (1999) but to show that seismicity following the July 26, 2001 event may be related to both strike-slip and normal faulting around Skyros. This is important in our hypothesis that the stress field varies at short distances (<30 km) in order to accommodate overall extensional strain (see Fig. 8 for model).

We computed static stress changes due to slip along the Skyros fault using the DLC code by R. Simpson (USGS). A fault model based on waveform modeling was adopted as in Zahradnik (2002) (see Table 1). Modeling parameters are summarized in Table 3. The NOA earthquake epicentre was used on the basis of network geometry. An isotropic elastic half-space is assumed to represent crustal rheology. First, the stress tensor is calculated on horizontal observation planes at 5 and 10 km depth on a 100 km \times 100 km grid surrounding the earthquake epicentre, with 1 km grid spacing. Then, we calculated the change in the Coulomb failure function (CFF) on both optimal and non-optimal failure planes (e.g. Reasenber and

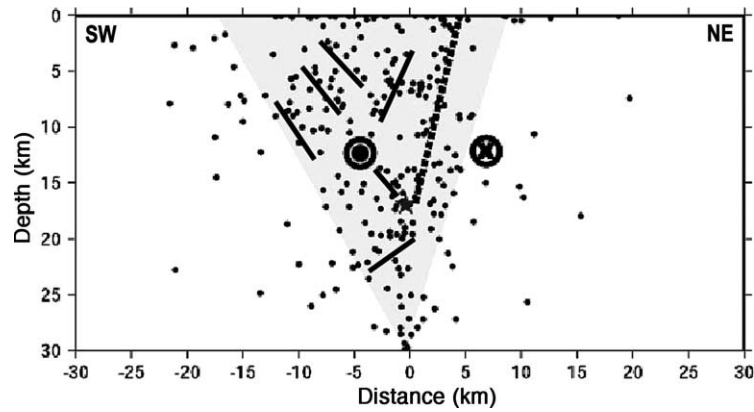


Fig. 5. Cross-section through the aftershock sequence, normal to the strike of Skyros fault. (⊗) indicates block motion away from the observer. Thick dashed line shows fault plane and thin black lines show smaller fault planes activated during the aftershock sequence. Star indicates mainshock.

Simpson, 1992).

$$\Delta\text{CFF} = \Delta\tau + \mu' \Delta\sigma \quad (1)$$

where $\Delta\tau$ is the coseismic change in shear stress in the direction of fault slip, $\Delta\sigma$ is the change in normal stress (with tension positive), and μ' is the effective coefficient of friction, accounting for pore-fluid pressure effects.

Following the stress tensor analysis (Fig. 4) the regional stress field was specified as East–West compression with a tectonic stress of 100 bar. The final stress field is the sum of the regional stress field and the stress changes generated by our model of the earthquake. We carried out calculations with a μ' value of 0.4 which is appropriate for large faults (Stein, 1999). Finally, we computed the ΔCFF on planes of fixed orientation which are likely to provide planes of failure. We found that the Skyros mainshock induced up to 5 bar of positive Coulomb change on the greater hypocentral region, which can be associated with aftershocks (Fig. 6). Less than 10 aftershocks have occurred in areas with less than 0.3 bars positive

Table 3
Input parameters used for stress transfer modeling

Poisson ratio	0.25
Shear modulus	$\mu = 300,000$ bar
Projection	UTM zone 35
Epicentre longitude	24.338
Epicentre latitude	39.046
Hypocentral depth	8 km
Fault strike/dip	150/70 SW
Rake angle	10
Fault length	20 km
Fault width	10 km
Earthquake magnitude	6.4 Mw
Strike-slip displacement	0.63 m
Dip-slip displacement	−0.115 m (up is reverse motion)

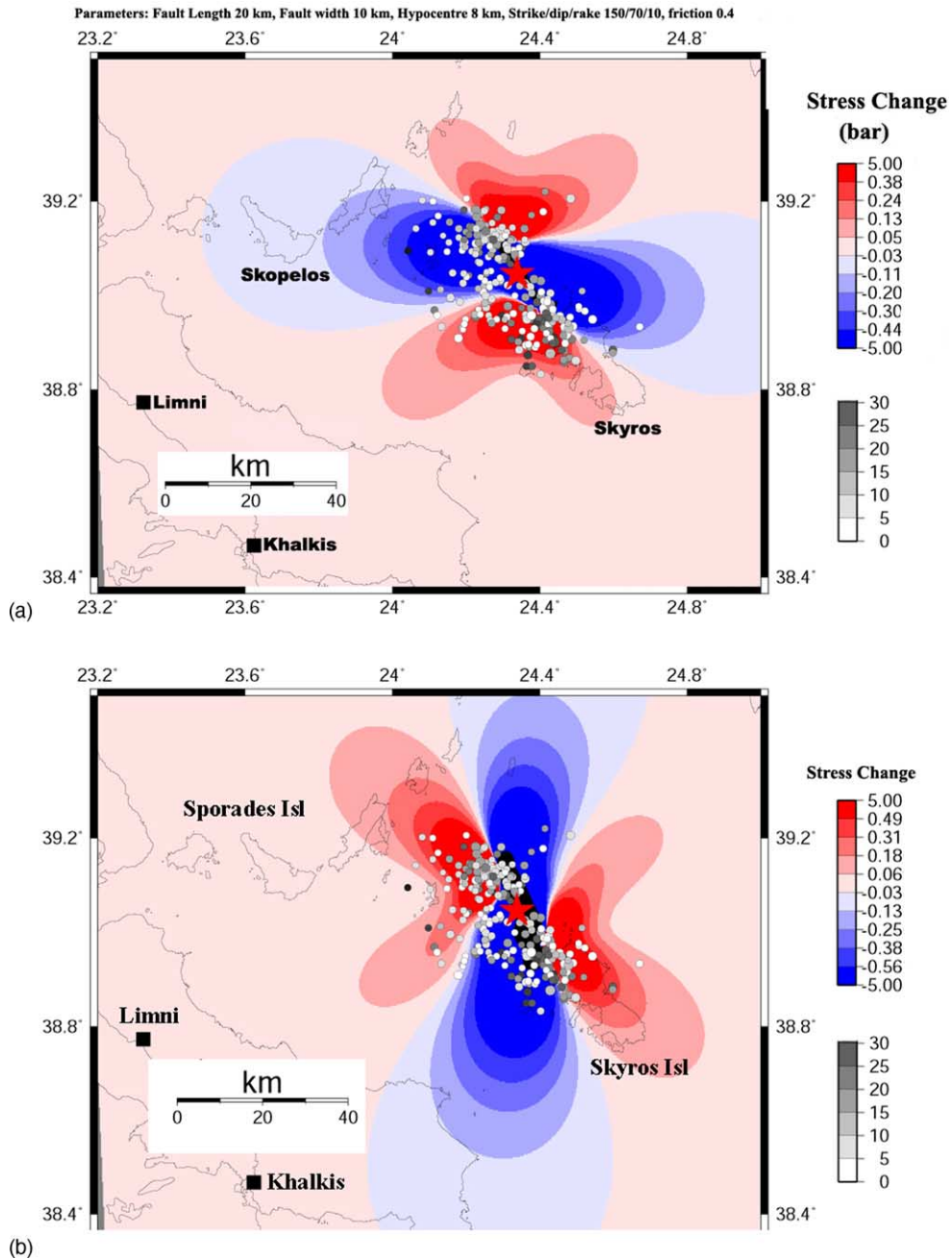


Fig. 6. Maps of co-seismic stress change showing how aftershock sequence fits the model of triggered seismicity. Red indicates positive stress change, blue the opposite. Coulomb stress is sampled at 5 km depth or half fault width. The effective coefficient of friction is 0.4. Grey legend indicates depth of hypocentre. Star shows the epicentre of the Mw 6.4 mainshock. (a) Δ CFF calculation on optimal failure planes for regional, East–West compression. (b) Δ CFF calculation on failure planes striking East–West, simulating normal faults at right angles to central Greece extension.

Δ CFF. Aftershocks were triggered as far as 25 km to the SE of the mainshock epicentre. Other studies of stress transfer (e.g. Harris, 1998; Stein, 1999) have indicated that similar Δ CFF levels are associated with aftershock triggering. In addition, the south cluster of aftershocks (Fig. 1) is almost entirely included within the positive stress lobe of the optimal planes scenario (Fig. 6a). However, most of the northern cluster of aftershocks falls outside the positive Δ CFF lobe of the optimal planes scenario. This result indicates failure along fault planes of different geometry and kinematics which may be modeled by a non-optimal configuration (Fig. 6b). Such failure planes may be provided by E–W striking normal faults due to the proximity of this region to the Greek mainland. Indeed it is reasonable to accept this hypothesis because the north aftershock cluster falls inside the positive Δ CFF stress lobe (Fig. 6b). We infer that normal faults exist at a distance 5–20 km to the northwest of mainshock epicentre and they required about 0.18 extra bar in order to slip after July 26, 00:29 GMT (Fig. 6b). In addition, our results indicate that the Skyros event has advanced rupture times of optimal faults to the North and South of the July 26, epicentre (Fig. 6a). On the contrary, optimal faults to the west and to the east have had their rupture times delayed due to a reduction on their stress levels. This change on stress levels may affect seismicity patterns in North Aegean as observed by Papadopoulos et al. (2002).

4. Tectonic implications

4.1. Fault length, age

The seismological data may be used to estimate fault length, fault displacement and fault age. On average, published source parameters for the Skyros earthquake suggest a 20 km length for the seismogenic fault (Table 1; Zahradnik, 2002; Karakostas et al., 2003). Assuming appropriate scaling relationships from geological data between maximum displacement D_{\max} and length L , as $D_{\max} = 0.03L^{1.06}$ (Schlische et al., 1996) we obtain a value of 718 m for cumulative strike-slip displacement. Mean slip rates in central Greece outside the Gulf of Corinth have been recently introduced from geological mapping (Caputo, 1993; Ganas et al., 1998; Pantosti et al., 2001; Ganas et al., 2004) and trenching (Pavlidis et al., 2003) as ranging between 0.2 and 0.5 mm per year. Assuming that the Skyros fault slip rate matches those slip rates, it follows that this fault is an Early Quaternary structure between 1.4 and 3.5 My old.

4.2. Spatial variation of stress

The map of focal plane solutions from large earthquakes occurred in the North-central Aegean area during the last 40 years (Fig. 7) shows that three types of faults are active: right-lateral strike-slip, left-lateral strike-slip and normal faults. We suggest that all these faults may be active despite the different kinematics due to slip partitioning. This process is controlled by the regional strain field, i.e. N–S extension. In terms of dynamics of the deformation this translates to a transitional area about 170 km wide in the central Aegean (Fig. 7). The eastern boundary is approximately at 25°E where E–W, horizontal compression dominates. The western boundary is at 23°E where the maximum compressive stress is vertical. In the space between, the principal stress axes σ_2 and σ_1 vary at distances less than 30 km. The transition is from a stress field characterized by vertical σ_2 to a vertical σ_1 with σ_3 trending roughly N10°E. The overall variation of the stress field is gradual as determined by the progressive predominance

rotated southwards with finite strain. However, there are two uncertainties in our analysis: (a) our stress tensor inversion is associated with 10° uncertainty in σ_1 orientation and (b) the fault plane orientation estimates range between $N128^\circ E$ and $N161^\circ E$ (Table 1). So the angle of rotation for the Skyros fault may lie between 8° and 38° according to the error bounds. In addition, because of the fault kinematics it is unlikely that this is a re-activated structure of Pliocene age (see Section 5). To summarize it is suggested that the Skyros fault formed as an intact fracture in Early Quaternary times and has rotated 18° with progressive strain to its present orientation.

5. Discussion

5.1. 1967 event

The bathymetry of the central Aegean shows the formation of an elongated basin offshore Skyros (15 km to the NE; Fig. 1), with a NW–SE orientation. This area hosted the 1967, M6.6 event (Table 4; Delibasis and Drakopoulos, 1974; Taymaz et al., 1991) whose digital waveform analysis indicates normal faulting striking NW–SE with the slip vector oriented $N1^\circ E$. It is reasonable to associate the 1967 earthquake with the scarp forming the western margin of the Skyros basin (Fig. 1), in agreement with Taymaz et al. (1991). Then, this normal-slip event occurs along a fault arranged en-echelon to the left-lateral Skyros fault. This earthquake may seem paradoxical to occur within an area dominated by strike-slip tectonics. However, we suggest that the 1967 event may be explained by the extension occurring at the ends of two, conjugate strike slip faults (Fig. 8). In that region, the crust moves to the NE because of right-lateral motion along the fault that hosted the 1981 earthquakes (Table 4; Taymaz et al., 1991). At the same time the crust moves also to the NW because of left-lateral motion along the Skyros fault. Therefore, the 1967 earthquake occurred along the western margin of the extensional basin, formed between two conjugate, strike-slip faults (Fig. 8).

Table 4

The parameters of the focal mechanisms of shallow earthquakes in the North-central Aegean Sea from 1965 onwards

Event date YYYY/MM/DD	Time GMT	Latitude	Longitude	Depth	Magnitude	Fault plane strike/dip/rake	Reference
1965/03/09	17:57:54	39.34	23.82	8	6.1 Ms	135/85/15	Taymaz et al. (1991)
1967/03/04	17:58:09	39.25	24.60	10	6.6 Ms	313/43/–56	Taymaz et al. (1991)
1968/02/19	22:45:42	39.40	24.94	15	7.0 Ms	311/90/20	Taymaz et al. (1991)
1980/07/09	02:11:57	39.30	22.90	10	6.5 Ms	81/40/–90	Papazachos et al. (1991)
1981/12/19	14:10:51	39.22	25.25	10	7.2 Ms	60/79/175	Taymaz et al. (1991)
1981/12/27	17:39:13	38.91	24.92	6	6.5 Ms	216/79/175	Taymaz et al. (1991)
1982/01/18	19:27:25	39.96	24.39	7	6.9 Ms	233/62/187	Taymaz et al. (1991)
1983/08/06	15:43:52	40.14	24.74	7	6.9 Ms	47/83/180	Taymaz et al. (1991)
1985/04/30	18:14:12	39.26	22.81	11	5.5 Ms	77/50/–105	Taymaz et al. (1991)
1999/02/07	22:28:34	38.73	23.37	17	4.8 Mw	85/35/–104	Pondrelli et al. (2002)
2000/08/22	03:35:38	39.50	23.78	10	5.0 Mw	286/41/–99	Pondrelli et al. (2002)
2001/07/26	00:21:39	39.06	24.35	16.9	6.5 Mw	150/70/10	Melis et al. (2001)
2001/12/07	19:44:52	39.33	23.75	7	5.5 Ms	50/85/–150	This study
2002/09/05	22:19:50	38.59	24.52	18	4.8 Mw	252/74/–164	Pondrelli et al. (2002)

Strike, dip, rake are in degrees. Depth is in km.

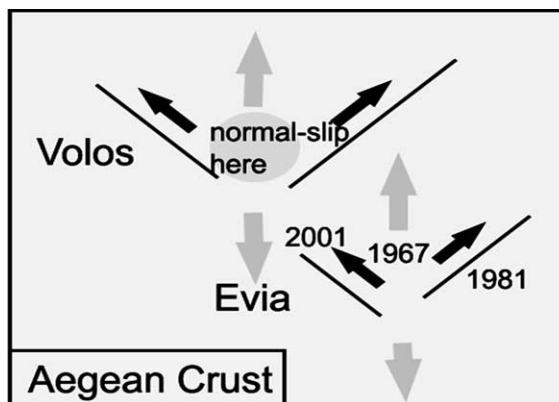


Fig. 8. Schematic diagram showing formation of extensional basins at ends of conjugate strike slip faults. Because the crust moves towards opposing directions normal faulting has to initiate in order to accommodate new space (gap). Not to scale.

5.2. Primary versus secondary origin

The NW–SE Skyros fault is a mature strike-slip structure accommodating strain for at least 1.5 My. The kinematics and geographic location of the fault may be explained by two hypotheses: (a) the fault acts as a R' shear (Pavlidis and Tranos, 1991; antithetic Reidel shear; i.e. secondary structure) within the overall right-lateral strike-slip regime (e.g. Wilcox et al., 1973) or (b) the fault is a primary, left-lateral structure oriented favorably to the E–W compression in central Aegean as it is suggested here. The E–W compression is imposed by the westward motion of the Anatolian block (e.g. Taymaz et al., 1991; Kahle et al., 2000). The first hypothesis may fit to models proposing linkage of the NAF strands in the Aegean to the normal faults of central Greece (e.g. Hatzfeld et al., 1999; Kiratzi, 2002; Kiratzi and Louvari, 2003). However, the existence of seismic slip along NW–SE faults as demonstrated by the 2001 event does not agree with such models. Faults as the one hosted the 2001 event penetrate the entire seismogenic crust (Fig. 5) and are structures 10–20 km long, thus forming barriers to geometric linkage across the Greek mainland's eastern coast. Although the instrumental seismicity records span a period of nearly 40 years, it is reasonable to suggest that other left-lateral faults may occur both to the NW of Skyros and to the SE, respectively (Fig. 7). For example, the linear form of the Pelion Mountain coastline may be indicative of such structure to the NW. Furthermore, it is suggested that extension in the Sporades basin (Fig. 7) may be also explained by the model of Fig. 8. Inside Sporades basin active normal faulting has a $N100^{\circ}E$ orientation (Laigle et al., 2000). This geometry seems appropriate to accommodate extension at the ends of conjugate, strike-slip faults. Therefore, it may be argued that the main NAF branch has not propagated in the area to the west of the 23.5° Meridian East.

5.3. Reactivation of old (Miocene) structures

It has been suggested (Koukouvelas and Aydin, 2002; Roumelioti et al., 2003) that the active, NW-striking structures in the North and central Aegean Sea may take advantage of favorably-oriented planes of weakness of Upper Miocene–Pliocene normal faults when the extension direction was NE–SW (Mercier

et al., 1989; Caputo and Pavlides, 1993; Galanakis et al., 1998) or of other older structures. Perhaps this model is appropriate for other parts of the Aegean but it does not apply to our study area in central Aegean. Our findings include kinematic evidence provided by the seismological data of the July 26, 2001 event that constrain active fault geometry. The focal plane solution of the earthquake showed that the plane dips steeply to the SW at 70° – 86° . (Table 1 and Fig. 5) and has a small reverse component. Such reverse motion is incompatible to occur along a plane of weakness represented by a graben-bounding normal fault of 5–10 My age because the latter should occupy a much gentler angle, of the order of 30 – 40° . This low angle is due to normal fault rotation about horizontal axis during finite deformation (Jackson and McKenzie, 1983). This analysis suggests that the Skyros fault is not a re-activated structure of Neogene age.

6. Conclusions

The Skyros earthquake took place in central Aegean, an area well monitored by NOA (Chouliaras and Stavrakakis, 2001) in terms of network geometry. Therefore, both mainshock and aftershock sequence parameters were well determined and permitted us to make a substantial tectonic interpretation. Our main findings may be summarized as follows:

- a) The T -axes data from 50 well-determined focal mechanisms indicate N–S extensional strain (Fig. 3; mean azimuth $N7^{\circ}E$). Stress tensor inversion of the same sequence showed that the maximum compressive stress (σ_1) is sub-horizontal at $N102^{\circ}E$ while σ_3 is oriented $N13^{\circ}E$. The extension direction agrees with geological data from the Gulf of Evia graben, where mean extension axis is directed $N14^{\circ}E$ (Roberts and Ganas, 2000).
- b) The Skyros left-lateral fault is a large Quaternary structure in the central Aegean crust blocking one of the North Anatolia Fault branches to propagate to the west. The fault initiated as a shear fracture with respect to regional horizontal compression ($N102^{\circ}E$) and it has rotated clockwise by $18^{\circ} \pm 10^{\circ}$.
- c) The stress field varies within a transitional area about 170 km wide in the central Aegean (Fig. 7). This stress variation is characterized by a switch of the vertical principal stress axis between σ_2 and σ_1 which is caused by the simultaneous operation of both conjugate strike-slip faults and of normal faults accommodating extension in newly-opened space in between the former faults (Fig. 8). This style of deformation marks the terminating influence of the North Anatolian Fault into the Aegean Sea.

Acknowledgements

We thank two anonymous reviewers and the Editor-in-Chief Giorgio Ranalli for comments and suggestions. We are indebted to Bob Simpson and Ruth Harris for their help in stress transfer theory. We also thank Gerassimos Papadopoulos and Maria Sachpazi, for discussions. Prof Billiris provided the Aegean bathymetry data. Funding was partially provided by the Earthquake Planning and Protection Organisation of Greece and by the General Secretariat for Research and Technology. Figures were prepared using the GMT software.

References

- Armijo, R., Meyer, B., Hubert, A., Barka, A., 1999. Westward propagation of the North Anatolian fault into the northern Aegean: timing and kinematics. *Geology* 27, 267–270.
- Barakou, Th., Delibasis, N., Voulgaris, N., Baier, B., 2001. Seismotectonic features in the northern Aegean Sea. *Bull. Geol. Soc. Greece* 34, 1449–1456.
- Benetatos, C., Rومelioti, Z., Kiratzi, A., Melis, N., 2002. Source parameters of the M 6.5 Skyros island (North Aegean Sea) earthquake July 26. *Ann. Geophys.* 45 (3), 513–526.
- Caputo, R., 1993. Morphotectonics and kinematics of the Tyrnavos Fault, northern Larissa Plain. *Greece Z. Geomorph. N. F.* 94 (Suppl. -Bd), 167–185.
- Caputo, R., Pavlides, S., 1993. Late Cenozoic geodynamic evolution of Thessaly and surroundings (central northern Greece). *Tectonophysics* 223 (3/4), 339–362.
- Chouliaras, G., Stavrakakis, G.N., 2001. Current seismic quiescence in Greece: implications for seismic hazard. *J. Seismol.* 5, 595–608.
- Delibasis, N., Drakopoulos, J., 1974. Focal mechanism of earthquakes in the North Aegean Sea. 1968 and related problems. In: *Proceedings of the XIIIth General Assembly of the European Seismological Commission (Part I)*, pp. 151–167.
- Drakatos, G., Stavrakakis, G., Ganas, A., Karastathis, V., Melis, N., Ziazia, M., Plessa, A., 2004. The 26 July 2001 Skyros (north Aegean Sea, Greece) earthquake. In: *Lekkas, E.L. (Eds.), Earthquake Geodynamics: Seismic Case Studies*, WIT Press Series. *Advances in Earthquake Engineering*, ISBN 1-85312-996-8, pp. 81–90.
- Galanakis, D., Pavlides, S.B., Mountrakis, D., 1998. Recent brittle tectonics in Almyros-Pagasitikos, Maliakos, N. Euboea & Pilio. *Bull. Geol. Soc. Greece* 32, 263–273.
- Ganas, A., Roberts, G.P., Memou, T., 1998. Segment boundaries, the 1894 ruptures and strain patterns along the Atalanti Fault, central Greece. *J. Geodyn.* 26, 461–486.
- Ganas, A., Pavlides, S.B., Sboras, S., Valkaniotis, S., Papaioannou, S., Alexandris, A.G., Plessa, A., Papadopoulos, G.A., 2004. Active fault geometry and kinematics in Parnitha Mountain, Attica. *Greece J. Struct. Geol.* 26, 2103–2118.
- Gephart, J., Forsyth, W., 1984. An improved method for determining the regional stress tensor using earthquake focal mechanism data: applications to the San Fernando earthquake sequence. *J. Geophys. Res.* 89, 9305–9320.
- Gephart, J., 1990. Stress and the direction of slip on fault planes. *Tectonics* 9, 845–858.
- Harris, R.A., 1998. Introduction to special section: stress triggers, stress shadows, and implications for seismic hazard. *J. Geophys. Res.* 103 (24), 347–24, 358.
- Hatzfeld, D., Ziazia, M., Kementzetzidou, D., Hatzidimitriou, P., Papagiorgopoulos, D., Makropoulos, K., Papadimitriou, P., Deschamps, A., 1999. Microseismicity and focal mechanisms at the western termination of the North Anatolian Fault and their implications for continental tectonics. *Geophys. J. Int.* 137, 891–908.
- Jackson, J.A., McKenzie, D.P., 1983. The geometrical evolution of normal fault systems. *J. Struct. Geol.* 5, 471–482.
- Kahle, H.-G., Cocard, m., Peter, Y., Geiger, A., Reilinger, R., Barka, A., Veis, G., 2000. GPS-derived strain rate field within the boundary zones of the Eurasian, African, and Arabian Plates. *J. Geophys. Res.* 105, 23353–23370.
- Karakostas, V.G., Papadimitriou, E.E., Karakaisis, G.F., Papazachos, C.B., Scordilis, E.M., Vargemezis, G., Aidona E., 2003. The 2001 Skyros, Northern Aegean, Greece, earthquake sequence: off-fault aftershocks, tectonic implications, and seismicity triggering. *Geophys. Res. Lett.* 30 (1), doi:10.1029/2002GL015814.
- Kiratzi, A.A., 2002. Stress tensor inversions along the northwestern North Anatolian Fault Zone and its continuation into the North Aegean Sea. *Geophys. J. Int.* 151, 360–376.
- Kiratzi, A., Louvari, E., 2003. Focal mechanisms of shallow earthquakes in the Aegean Sea and the surrounding lands determined by waveform modelling: a new database. *J. Geodyn.* 36 (1–2), 251–274.
- Koukouvelas, I.K., Aydin, A., 2002. Fault structure and related basins of the North Aegean Sea and its surroundings. *Tectonics* 21, 1046, doi:10.1029/2001TC901037.
- Laigle, M., Hirn, A., Sachpazi, M., Roussos, N., 2000. North Aegean crustal deformation: an active fault imaged to 10 km depth by reflection seismic data. *Geology* 28, 71–74.
- Makris, J., Veis, R., 1977. Crustal structure of the Aegean Sea and the islands of Evia and Crete, Greece, obtained by refraction seismic experiments. *J. Geophys.* 42, 329–341.
- Melis, N.S., Stavrakakis, G.N., Zahradnik, J., 2001. A study of the focal properties of the Skyros earthquake (MW = 6.5/July 26, 2001), Aegean Sea. *Greece Orfeus Newslett.* 3, 11.

- Mercier, J.L., Sorel, D., Vergely, P., Simeakis, K., 1989. Extensional tectonic regimes in the Aegean basins during the Cenozoic. *Basin Res.* 2, 49–71.
- Nur, A., Ron, H., Scotti, O., 1986. Fault mechanics and the kinematics of block rotations. *Geology* 14, 746–749.
- Pantosti, D., De Martini, P.M., Papanastassiou, D., Palyvos, N., Lemeille, F., Stavrakakis, G., 2001. A Reappraisal of the 1894 Atalanti earthquake surface ruptures, Central Greece. *Bull. Seismol. Soc. Am.* 91, 760–780.
- Papadopoulos, G.A., Ganas, A., Plessa, A., 2002. The Skyros earthquake (Mw 6.5) of 26 July 2001 and precursory seismicity patterns in the North Aegean Sea. *Bull. Seismol. Soc. Am.* 92 (3), 1141–1145.
- Papazachos, B., Kiratzi, A., Papadimitriou, E., 1991. Regional focal mechanisms for earthquakes in the Aegean area. *Pure Appl. Geophys.* 136, 405–420.
- Pavlidis, S.B., Tranos, M.D., 1991. Structural characteristics of two strong earthquakes in the North Aegean: Ierissos (1932) and Agios Efstratios (1968). *J. Struct. Geol.* 13, 205–214.
- Pavlidis, S.B., Koukouvelas, I., Ganas, A., Kokkalas, S., Tsodoulos, I., Stamatopoulos, L., Gountromichou, C., Valkaniotis, S., 2003. Preliminary palaeoseismological results from the Kaparelli. *Geophysical Research Abstracts*, vol. 5, 07069. Nice, European Geophysical Society.
- Pondrelli, S., Morelli, A., Ekström, G., Mazza, S., Boschi, E., Dziewonski, A.M., 2002. European-Mediterranean regional centroid-moment tensors: 1997–2000. *Phys. Earth Planet. Int.* 130, 71–101.
- Reasenber, P.A., Simpson, R.W., 1992. Response of regional seismicity to the static stress change produced by the Loma Prieta earthquake. *Science* 255, 1687–1690.
- Roberts, G.P., Ganas, A., 2000. Fault-slip directions in central and southern Greece measured from striated and corrugated fault planes: comparison with focal mechanism and geodetic data. *J. Geophys. Res.* 105 (B10), 23443–23462.
- Roumelioti, Z., Kiratzi, A., Melis, N., 2003. Relocation of the 26 July 2001 Skyros Island (Greece) earthquake sequence using the double-difference technique. *Phys. Earth Planet. Interiors* 138 (3–4), 231–239.
- Roumelioti, Z., Kiratzi, A., Dreger, D., 2004. The source process of the 2001 July 26 Skyros Island (Greece) earthquake. *Geophys. J. Int.* 156 (3), 541–548.
- Schlische, R.W., Young, S.S., Ackermann, R.V., Gupta, A., 1996. Geometry and scaling relations of a population of very small rift-related faults. *Geology* 24, 683–686.
- Scholtz, C.H., 1990. *The Mechanics of Earthquake and Faulting*. Cambridge University Press, p. 439.
- Stein, R.S., 1999. The role of stress transfer in earthquake occurrence. *Nature* 402, 605–609.
- Taymaz, T., Jackson, J., McKenzie, D., 1991. Active tectonics of the north and central Aegean Sea. *Geophys. J. Int.* 106, 433–490.
- Tsokas, G.N., Hansen, R.O., 1997. Study of the crustal thickness and the subducting lithosphere in Greece from gravity data. *J. Geophys. Res.* 102, 20585–20597.
- Wiemer, S., Zuniga, R.F., 1994. ZMAP—a software package to analyze seismicity. *EOS Trans.* 75, 456.
- Wilcox, R.E., Harding, T.P., Seely, D.R., 1973. Basic wrench tectonics. *AAPG Bull.* 57, 74–96.
- Zahradnik, J., 2002. The weak-motion modeling of the Skyros island, Aegean Sea Mw = 6. 5 earthquake of July 26. *Studia Geophys. Geodaet.* 46, 753–771.